Chapter 13

Production of Electroweak Bosons at Hadron Colliders: Theoretical Aspects

Michelangelo L. Mangano

CERN, TH Department, 1211 Geneva 23, Switzerland
michelangelo.mangano@cern.ch

Since the $W^{\pm}$ and Z^0 discovery, hadron colliders have provided a fertile ground, in which continuously improving measurements and theoretical predictions allow to precisely determine the gauge boson properties, and to probe the dynamics of electroweak and strong interactions. This article will review, from a theoretical perspective, the role played by the study, at hadron colliders, of electroweak boson production properties, from the better understanding of the proton structure, to the discovery and studies of the top quark and of the Higgs, to the searches for new phenomena beyond the Standard Model.

1. Introduction

All bosons of the electroweak (EW) sector of the Standard Model (SM), namely the gauge vector bosons $W^{\pm}$ and Z^0, and the scalar Higgs boson H^0, have been discovered at hadron colliders.[1–6] This well known fact is sufficient to underscore in the strongest terms the key role played by hadron colliders in the exploration of the EW sector of the SM.

In hadron colliders, the physics of EW gauge bosons has many facets. The abundant production rates via the Drell–Yan (DY) process[7] enables significant measurements of their properties, the best example being the so far unparalleled precision of the determination of the W boson mass, M_W, obtained at the Tevatron.[8] The production of EW gauge bosons in the decays of the top quark and of the Higgs boson, furthermore, makes them indispensable tools in the study of the properties of these particles. The presence of W and Z bosons in the final state of a hadronic production process acts as a tag of the underlying dynamics, singling out a limited number of production channels, which can then be studied with great precision, due to the experimental cleanness of the leptonic decay modes, and thanks to the high accuracy achieved by the theoretical calculations. Last but not least, W and Z bosons appear as final or intermediate states in the decay of most particles predicted

in theories beyond the SM (BSM). Examples include the heavy bosons of new gauge interactions, supersymmetric particles, or heavy resonances featured in models of EW symmetry breaking alternative to the SM. The theoretical study and the measurements of EW gauge bosons are therefore a primary ingredient in the physics programme of hadron colliders.

It is impossible to provide, in this contribution, a complete historical overview of the development of this field, and to properly acknowledge the main contributions to both theoretical and experimental developments: on one side there are too many to fit in these few pages; on the other, the field is undergoing a continuous development, thanks to the multitude of new data that are arising from the LHC and to the rapid theoretical progress. Each of the topics briefly touched upon in this review is examined in the theoretical and experimental literature with a great degree of sophistication, and only an extended discussion would fully address the complexity and ramifications of their theoretical implications. In this review, I shall therefore limit myself to expose the great diversity of gauge boson physics in hadron collisions, through the qualitative discussion of the main ideas and results. Furthermore, I shall only cover the physics of vector gauge bosons, since the Higgs boson is covered in other chapters of this book.

I shall start from the general properties of inclusive W and Z production, focusing on the transverse and longitudinal dynamics and on the implications for the knowledge of the partonic content of the proton. I shall then discuss the phenomenological interest in the production of multiple gauge bosons. Finally, I shall overview the various mechanisms of associated production of gauge bosons and other SM particles, namely jets and heavy quarks.

2. QCD Aspects of Inclusive Vector Boson Production

The main feature of inclusive gauge boson production in hadronic collisions is that the leading-order (LO) amplitude, describing the elementary process $q\bar{q}^{(')} \to V$ $(V = W, Z)$ is purely EW. The dynamics of strong interactions, at this order, only enters indirectly through the parton distribution functions (PDFs), which parameterise in a phenomenological way the quark and gluon content of the proton.[a] At the large momentum scales typical of gauge boson production ($Q \sim M_V$), higher-order perturbative QCD corrections to the inclusive production are proportional to $\alpha_s(Q)$ and are typically small, in the range of 10–20%. They are known[9,10] today to next-to-next-to-leading order (NNLO), including the description of the differential distributions of the boson and of its decay leptons,[11–14] leaving theoretical uncertainties from higher-order QCD effects at the percent level. These results have been

---

[a]For the overview of the principles and tools of perturbative QCD and of the parton models, which are relevant to the physics of hadronic collisions, I refer to the Chapter in this Book by R. K. Ellis.

incorporated in full Monte Carlo calculations including the shower evolution, to give a complete description of the physical final states.[15–17] Next-to-leading-order (NLO) EW corrections are also known,[18–21] and play an important role both for precision measurements, and in the production rate of dilepton pairs at large p_T or with large mass, above the TeV, where they can be larger than 10%. Finally, progress towards a complete calculation of the mixed $\mathcal{O}(\alpha_s\alpha)$ corrections has been recently reported in Ref. 22.

When considering the first and second generation quarks that dominate the production of W and Z bosons, their weak couplings, including the CKM mixing parameters, are known experimentally with a precision better than a percent. This exceeds the accuracy of possible measurements in hadronic collisions, indicating that such measurements could not be possibly affected, at this level of precision, by the presence of new physics phenomena. They therefore provide an excellent ground to probe to percent precision the effects of higher-order QCD corrections and of PDFs.[23] To be more explicit, consider the leading-order (LO) cross section given by:

$$d\sigma(h_1 h_2 \to V + X) = \int dx_1 \ dx_2 \sum_{i,j} f_i(x_1, Q) \ f_j(x_2.Q) \ d\hat{\sigma}(ij \to V), \qquad (1)$$

where $x_{1,2}$ are the fractions of the hadrons momenta and $f_{i,j}$ are the corresponding distributions of (anti)quark flavours (i, j). In the case of W production (a similar result holds for the Z), the LO partonic cross section is given by:

$$\hat{\sigma}(q_i \bar{q}_j \to W) = \pi \ \frac{\sqrt{2}}{3} \ |V_{ij}|^2 \ G_F \ M_W^2 \ \delta(\hat{s} - M_W^2) = A_{ij} M_W^2 \ \delta(\hat{s} - M_W^2). \qquad (2)$$

Here $\hat{s} = x_1 x_2 S$ is the partonic centre-of-mass energy squared, and V_{ij} is the element of the Cabibbo–Kobayashi–Maskawa (CKM) matrix.

Written in terms of $\tau = x_1 x_2$ and of the rapidity $y = \log[(E_W + p_W^z)/(E_W - p_W^z)]^{1/2} \equiv \log(x_1/x_2)^{1/2}$, the differential and total cross sections are given by:

$$\frac{d\sigma_W}{dy} = \sum_{i,j} \frac{\pi A_{ij}}{M_W^2} \tau \ f_i(x_1) \ f_j(x_2), \quad x_{1,2} = \sqrt{\tau} e^{\pm y}, \qquad (3)$$

$$\sigma_W = \sum_{i,j} \frac{\pi A_{ij}}{M_W^2} \tau \int_\tau^1 \frac{dx}{x} \ f_i(x) \ f_j\left(\frac{\tau}{x}\right) \equiv \sum_{i,j} \frac{\pi A_{ij}}{M_W^2} \tau L_{ij}(\tau) \qquad (4)$$

where the function $L_{ij}(\tau)$ is usually called *partonic luminosity*. In the case of $u\bar{d}$ collisions, $\frac{\pi A_{ij}}{M_W^2} \sim 6.5$ nb. It is interesting to study the partonic luminosity as a function of the hadronic centre-of-mass energy. This can be done by taking a simple approximation for the parton densities. Using the approximate behaviour $f_i(x) \sim 1/x^{1+\delta}$,

with $\delta < 1$, one easily obtains:

$$L(\tau) = \frac{1}{\tau^{1+\delta}} \, \log\left(\frac{1}{\tau}\right) \quad \text{and} \quad \sigma_W \propto \left(\frac{S}{M_W^2}\right)^{\delta} \log\left(\frac{S}{M_W^2}\right). \tag{5}$$

The gauge boson production cross section grows therefore at least logarithmically with the hadronic centre-of-mass energy.

2.1. *Rapidity spectrum of W and Z bosons*

The features of the momentum distribution of vector bosons along the beam direction (z) are mostly controlled by properties of the parton PDFs. In particular, in the case of W bosons, the differences between the PDFs of up- and down-type quarks and antiquarks lead to interesting production asymmetries. Since the measurement of asymmetries is typically very accurate, due to the cancellation of many experimental and theoretical uncertainties, these play a fundamental role in the precision determination of quark and antiquark PDFs. Furthermore, the production asymmetries are modulated by the parity violation of the vector boson couplings, leading to further handles for the discrimination of quark and antiquark densities, and inducing a sensitivity to the weak mixing angle $\sin^2 \theta_{\text{eff}}^{\text{lept}}$, which controls the vector and axial components of Z boson interactions.

2.1.1. *W charge asymmetries*

For $p\bar{p}$ collisions, and assuming for simplicity the dominance of u and d quarks, we have:

$$\frac{d\sigma_{W^+}}{dy} \propto f_u^p(x_1) \, f_{\bar{d}}^{\bar{p}}(x_2) + f_{\bar{d}}^p(x_1) f_u^{\bar{p}}(x_2), \tag{6}$$

$$\frac{d\sigma_{W^-}}{dy} \propto f_{\bar{u}}^p(x_1) \, f_d^{\bar{p}}(x_2) + f_d^p(x_1) f_{\bar{u}}^{\bar{p}}(x_2). \tag{7}$$

We can then construct the following charge asymmetry (using $f_q^{\bar{p}} = f_{\bar{q}}^p$ and assuming the dominance of the quark densities over the antiquark ones, which is valid in the kinematical region of interest for W production at the Tevatron):

$$A(y) = -A(-y) = \frac{\frac{d\sigma_{W^+}}{dy} - \frac{d\sigma_{W^-}}{dy}}{\frac{d\sigma_{W^+}}{dy} + \frac{d\sigma_{W^-}}{dy}} \sim \frac{f_u^p(x_1) \, f_d^p(x_2) - f_d^p(x_1) \, f_u^p(x_2)}{f_u^p(x_1) \, f_d^p(x_2) + f_d^p(x_1) \, f_u^p(x_2)}. \tag{8}$$

Setting $f_u(x) = f_d(x)R(x)$ we then get:

$$A(y) \sim \frac{R(x_1) - R(x_2)}{R(x_1) + R(x_2)}, \tag{9}$$

which gives an explicit relation between asymmetry and the functional dependence of the $u(x)/d(x)$ ratio. This ratio is close to 1 at small x, where the quark distributions arise mostly from sea quarks, and it increases at larger x, where the valence contribution dominates. At positive y, where $x_1 > x_2$, we therefore expect a positive asymmetry. This is confirmed in the left plot of Fig. 2, showing the asymmetry measured at the Tevatron by the CDF experiment,[27] and compared to the NNLO QCD prediction[13,21,28,29] and an estimate of the PDF uncertainty. When measuring the charged lepton from W decay, the W production asymmetry is however modulated by the W decay asymmetry caused by parity violation. The squared amplitude for the process $f_1\bar{f}_2 \to W \to f_3\bar{f}_4$ is proportional to $(p_1 \cdot p_4)(p_2 \cdot p_3)$, where $f_{1,3}$ are fermions and $f_{2,4}$ antifermions, of momenta $p_{1,...,4}$. In the rest frame of this process, this is proportional to $(1 + \cos\theta)^2$, where θ is the scattering angle between final- and initial-state fermions. The momentum of the final-state fermion, therefore, points preferentially in the direction of the initial-state fermion's momentum, $\cos\theta \to 1$. For $d\bar{u} \to W^- \to \ell^-\bar{\nu}$ the charged lepton (a fermion) is more likely to move in the direction of the d quark, while for $u\bar{d} \to W^+ \to \ell^+\nu$ the charged lepton (an antifermion) is more likely to move backward. The rapidity distribution of charged leptons is therefore subject to a tension between the W production asymmetry, which at positive rapidity favours W^+ over W^-, and the decay asymmetry, which at positive rapidity favours ℓ^- over ℓ^+. The net result is a distribution that changes sign, becoming negative at large lepton rapidity. This is seen explicitly in the right plot of Fig. 2, from the D0 experiment,[30] which also shows the great sensitivity of this quantity to different PDF parameterisations, and the potential to improve their determination.
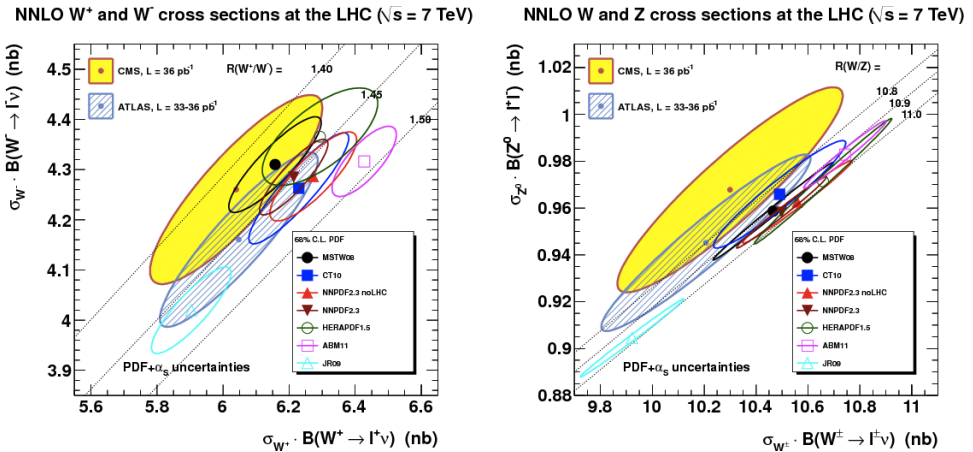

Fig. 1. W and Z boson cross sections in pp collisions at $\sqrt{S} = 7$ TeV: ATLAS[24] and CMS[25] data, compared to NNLO predictions for various PDF sets.[23]
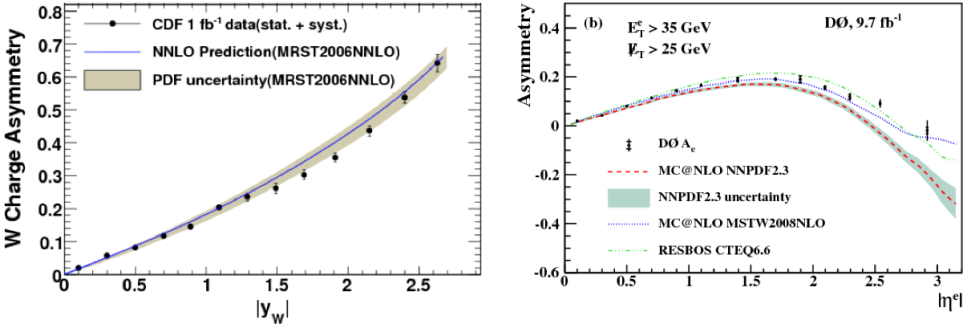
Fig. 2.   Production[27] (left) and leptonic[30] (right) charge asymmetries of W bosons in $p\bar{p}$ collisions at the Tevatron, $\sqrt{S} = 1.96\,\mathrm{TeV}$.
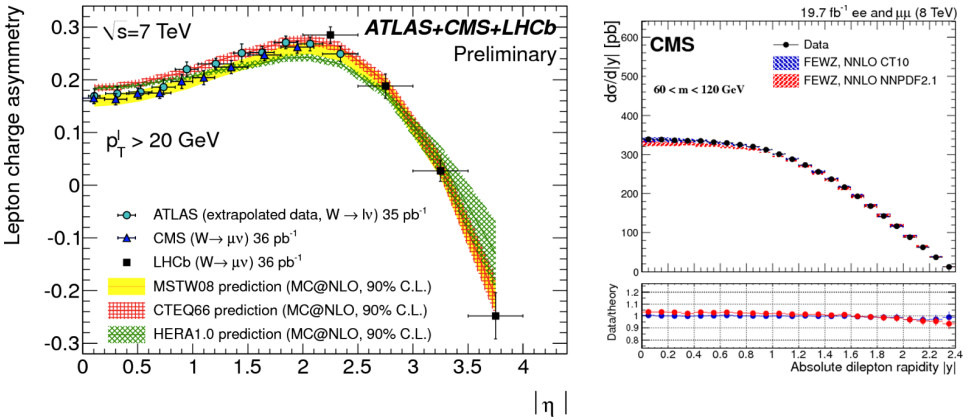

Fig. 3.   Left: leptonic charge asymmetries in W production at the LHC ($\sqrt{S} = 7$ TeV), extracted from the measurements of the ATLAS,[31] CMS[32] and LHCb[26] experiments. Right: Z boson rapidity spectrum from CMS,[33] compared with NNLO predictions.[21]

In pp collisions, assuming again the dominance of the first generation of quarks and $f_q^p(x) \gg f_{\bar{q}}^p(x)$ $(q = u, d)$ at large x, the W charge asymmetry takes the form:[b]

$$A(y) = A(-y) \sim \frac{R(x_{\max}) - r(x_{\min})}{R(x_{\max}) + r(x_{\min})}, \tag{10}$$

where $x_{\max(\min)} = \max(\min)(x_1, x_2)$ and $f_{\bar{u}}^p(x) = r(x) f_{\bar{d}}^p(x)$. The extended rapidity coverage offered by the combination of the ATLAS, CMS and LHCb detectors at the LHC, allows to fully exploit the potential of asymmetry measurements as a probe of the proton structure. This is highlighted in the left plot of Fig. 3, which summarises the LHC experimental results for the lepton charge asymmetry,

---

[b]It goes without saying that in actual analyses the contributions of all quark and antiquark flavours are taken into account. At the LHC, in particular, the contribution of strange and charm quarks is significant for the $W^{\pm}$ production rate, at the level of $\sim 30\%$.

obtained at $\sqrt{S} = 7$ TeV, compared to the theoretical predictions based on several sets of PDFs. In particular, notice the large spread of predictions in the largest rapidity regions, spread to be reduced once these data are included as new constraints in global PDF fits (see for example Refs. 34–37). The PDF sensitivity can be further enhanced by considering the W asymmetry at large rapidity in events produced in association with a high-p_T jet, as discussed in Ref. 38.

2.1.2. *Z rapidity spectrum and lepton charge asymmetries*

The measurement of the Z rapidity spectrum is very accurate, due to the precise reconstruction of its decay leptons. A comparison between CMS data[33] and the NNLO theoretical calculation is shown in the right plot of Fig. 3. The agreement is excellent, at the level of $\pm 5\%$, and on this scale one can detect differences between the two choices of PDFs, CT10[40] and NNPDF2.1,[39] confirming the power of these measurements to improve our knowledge of the quark distributions. Further inputs will arise from the Z production measurements performed by LHCb,[41–43] in the range $2 < y_Z < 4.25$.

As discussed above, parity violation effects lead to particular correlations in the decay directions of the final- and initial-state fermions. For Z^0 production, these correlations depend on the value of the weak mixing angle $\sin^2 \theta_{\text{eff}}^{\text{lept}}$, which parameterises the relative strength of vector and axial couplings. In $e^+ e^-$ collisions at the Z pole, the measurement of these correlations is in principle straightforward, since we know which of the initial state particles is a fermion. The combination of such measurements, done at LEP and SLC using both leptonic and b-quark Z decays, and in particular using at SLC polarised electron beams, led[44] to the very precise determination of $\sin^2 \theta_{\text{eff}}^{\text{lept}} = 0.23153 \pm 0.00016$. These measurements remain nevertheless puzzling, in view of a discrepancy between two of the most precise inputs into the global average, namely LEP's measurement of the forward–backward asymmetry of b quarks ($A_{\text{FB}}^{0,b}$), $\sin^2 \theta_{\text{eff}}^{\text{lept}} = 0.23221 \pm 0.00029$, and SLD's measurement of the polarised leptonic left–right asymmetry (A_{LR}), $\sin^2 \theta_{\text{eff}}^{\text{lept}} = 0.23098 \pm 0.00026$.

Due to the large statistics of Z bosons, experiments at hadron colliders have the potential to contribute to these measurements, and to address this puzzle. In practice, things are complicated by the lack of information, on a event-by-event basis, on which of the two initial-state partons is the quark, which is the antiquark, and what is their flavour (note that the initial state could also be qg, giving a different leptonic angular distribution). The problem is less severe in $p\bar{p}$ collisions than in pp collisions: in the former case, the most likely initial-state configuration has the quark coming from the p direction, and the antiquark coming from the $\bar{p}$ direction. A residual ambiguity remains, on whether the quark is of *up*-type or *down*-type, leading to a further slight dilution of the sensitivity. The CDF and D0 experiments at the Tevatron have presented the measurement of the weak mixing

angle, from the analysis of their full dataset of Z decays (in the muonic channel for CDF, and electronic channel for D0). CDF published[45] $\sin^2 \theta_{\text{eff}}^{\text{lept}} = 0.2315 \pm 0.0010$. D0 reports[46] $\sin^2 \theta_{\text{eff}}^{\text{lept}} = 0.21106 \pm 0.00053$, with individual contributions of ± 0.0004 from statistics and ± 0.0003 from the PDFs. This is the most precise measurement from hadronic colliders to date, with an overall uncertainty less than a factor of 2 larger than the individual $A_{\text{FB}}^{0,b}$ and A_{LR} determinations from LEP and SLD. These Tevatron measurements are consistent with the overall LEP+SLD average.

At the LHC, the extraction of the asymmetry is complicated by the reduced discrimination between the $q\bar{q}$ and the $\bar{q}q$ initial states, since both beams are protons. This reduced sensitivity is partly alleviated when considering events in which the Z boson is strongly boosted in either the forward or backward directions, since in this case it is more likely that the quark moves in the direction of the boosted Z, and that it is a u rather than a d. The extended rapidity coverage of the ATLAS and CMS experiments, and in particular the very forward coverage of LHCb, allows these measurements. The first result was reported by CMS,[47] based on the analysis of 1.1fb^{-1} of data at 7 TeV: $\sin^2 \theta_{\text{eff}}^{\text{lept}} = 0.2287 \pm 0.0020(\text{stat}) \pm 0.0025(\text{syst})$. ATLAS[48] published a result based on the full 4.8fb^{-1} 7 TeV dataset: $\sin^2 \theta_{\text{eff}}^{\text{lept}} = 0.2308 \pm 0.0005(\text{stat}) \pm 0.0006(\text{syst}) \pm 0.0009(\text{PDF}) = 0.2308 \pm 0.0012$. LHCb combined their measurements at both 7 and 8 TeV,[49] to obtain $\sin^2 \theta_{\text{eff}}^{\text{lept}} = 0.23142 \pm 0.00073(\text{stat}) \pm 0.00052(\text{syst}) \pm 0.00056(\text{theory}) = 0.2314 \pm 0.0011$, where the theoretical uncertainty arises mostly from the PDF uncertainty. The size of the PDF systematics in both ATLAS and LHCb results underscores the importance of future progress that should emerge from the ongoing PDF determination programme,[50] based on LHC data. Current estimates suggest that the LHC experiments should eventually reach systematics at the level of today's world average uncertainty.

2.2. *Transverse momentum spectrum*

When QCD corrections to inclusive gauge boson production are considered, the most notable effect is the appearance of a transverse momentum, $p_{T,V}$. This is the result of parton-level processes such as $q\bar{q} \to Vg$ and $qg \to qV$. The former are typically dominant in $p\bar{p}$ collisions, the latter in pp collisions, as shown in Fig. 4. Depending on the value of $p_{T,V}$, relative to M_V, different dynamical and theoretical issues are exposed, as summarised in this Section.

The spectrum at small p_T is dominated by the multiple emission of soft gluons (soft with respect to the hard scale of the process, namely M_V). This leads to corrections to $d\sigma/dp_{T,V}^2$ proportional to $1/p_{T,V}^2 \, \alpha_S^n \log^m(M_V/p_{T,V})$ (where n is the number of soft gluons emitted, and $m \leq 2n - 1$), which need to be resummed.[54–57] The leading-logarithmic soft-gluon resummation has been implemented in the context of the exact fixed-order NLO calculation,[62–65] and by now it has been extended to next-to-next-to-leading logarithmic accuracy (NNLL). For the most recent results, and a review of the existing literature on resummation, see Ref. 66.
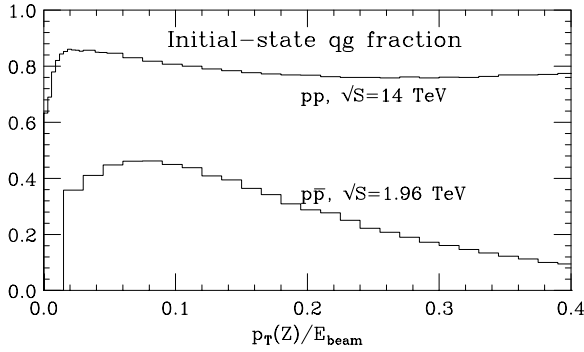
Fig. 4.   Fraction of the Z bosons of transverse momentum $p_T(Z)$ produced by the quark–gluon initial state, at the Tevatron and LHC.

At the lowest end, where $p_T \sim \mathcal{O}(\mathrm{GeV})$, the comparison of data with LO theoretical calculations has historically required the introduction of a modelling for the non-perturbative Fermi motion inside the hadron.[58] Most recently, the inclusion of exact higher-order perturbative effects up to the next-to-leading order and the resummation[59,60] of leading and sub-leading logarithms of p_T/M_V greatly reduced the need to introduce a phenomenological parameterisation of Fermi motion.[61]

The production dynamics for $p_{T,V}$ of $\mathcal{O}(M_V)$ and beyond is mostly controlled by purely perturbative physics, in addition of course to the required knowledge of the partonic densities of the proton. The comparison of data with theoretical predictions can therefore be used to improve the determination of the PDFs. The QCD corrections are known up to NLO,[62,64,65] and work is in progress towards a full NNLO result. In pp collisions the dominant process for high-p_T vector boson production is the Compton-like scattering $qg \to q'V$, as shown in Fig. 4 for the Z boson. This makes this process particularly sensitive to the gluon PDF, over a very large range of x values, as discussed in detail in Ref. 67. Such measurements should lead in the future to a more accurate determination of the gluon PDF, an essential step towards improving the precision of theoretical predictions for the total production rate of Higgs bosons.

Figure 5 shows the recent ATLAS results,[68] compared to theory, for the Z spectrum at $\sqrt{S} = 7$ TeV (similar results at 8 TeV have been reported by CMS).[69] Notice the reach of the measurement, extending up to p_T values of several hundred GeV, covering five orders of magnitude in rate. The upper right plot compares, on a linear scale, data and the results of NNLO QCD[13,21] (NNLO here and in Fig. 5 refers to $\mathcal{O}(\alpha_s^2)$, namely NNLO for the inclusive rate, but NLO for production at finite p_T). In the region of $p_T \gtrsim 20$ GeV, where the effect of the small-p_T logarithms discussed earlier is formally suppressed, data and theory agree to within 10%. At large p_T, 10% differences arise when changing the functional form of the renormalisation scale μ, from $\mu = M_W$ to $\mu = \sqrt{M_W^2 + p_{TW}^2}$. Notice also the non-negligible effect of NLO EW corrections,[72] which grow at large p_T. For smaller p_T
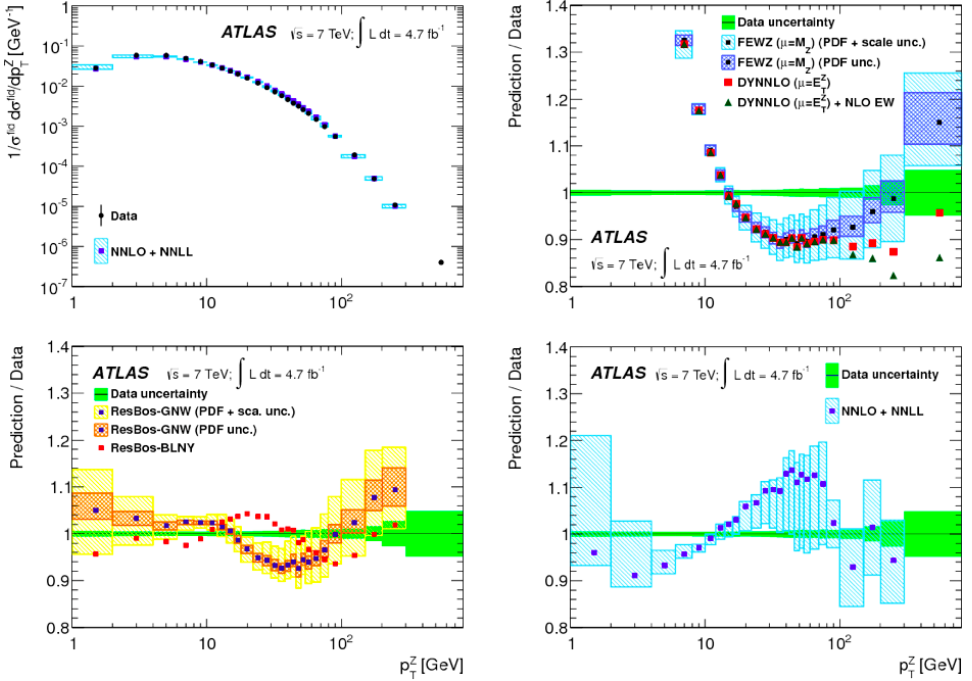
Fig. 5. Z boson p_T spectrum measured by ATLAS[68] (upper left), compared to various theoretical predictions: fixed-order NNLO (with different scales and with/without NLO EW corrections, upper right), resummed (N)NLO+(N)NLL (left[58,70] and right[71] lower plots).

values, where the fixed-order calculation is insufficient, a better agreement with the data shape is obtained by including the logarithmic resummation, an improvement included in the theoretical predictions shown in the bottom two plots. Overall, this comparison shows features in the pattern of the comparison between data and theory, and between different theoretical predictions, suggesting the need for further improvements before these very precise data can be used, for example, for improved determinations of the PDFs. Nevertheless, one should appreciate that the overall scale of deviations, which are compatible with the quoted uncertainties, is of order $\pm 10\%$, which remains quite impressive for a process in hadronic collisions.

2.3.   *Off-shell gauge-boson production at large invariant mass*

The study of large-mass DY pairs is the primary probe in the search for new interactions, characterised by the existence of heavy Z' (W'), and detectable as resonances (or jacobian peaks) in the $\ell^+\ell^-$ mass (or $\ell\nu$ transverse mass) spectra. This process, furthermore, tests the pointlike nature of quarks and leptons or the possible existence of contact interactions, mediated by heavy states beyond the reach of on-shell production. In this case, BSM signals would appear as smooth deviations w.r.t. the SM behaviour in the tails of the mass spectrum. Interpreting such deviations
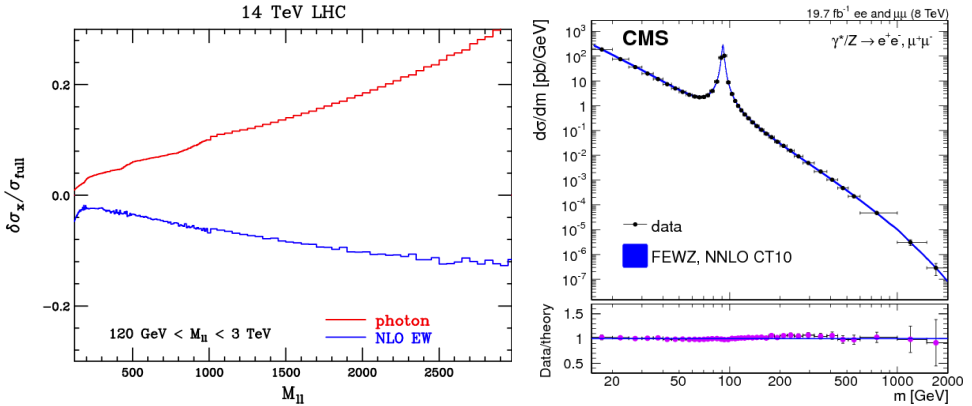
Fig. 6. Left: impact of EW and $\gamma\gamma \to \ell^+\ell^-$ corrections[75] on the DY mass spectrum at $\sqrt{S} = 14$ TeV. Right: Drell–Yan mass spectra in pp collisions at $\sqrt{S} = 8$ TeV,[33] compared against the theoretical prediction[75] including NNLO QCD and NLO EW corrections, with PDFs from Ref. 40.

requires a reliable control of the SM prediction, including the precise knowledge of PDFs and of higher-order QCD and EW effects, including, as recently emphasised in the literature, of purely QED processes such as $\gamma\gamma \to \ell^+\ell^-$, which require as input the knowledge of the photon density inside the proton. An example of the impact of NLO EW and of the $\gamma\gamma$ corrections is given in Fig. 6, obtained in Ref. 75 using the photon PDF from the NNPDF analysis.[76] Notice the large compensation between the two opposite-sign contributions. Notice also that the $\gamma\gamma$ channel is particularly large for this observable, since the DY pair here is allowed to have small p_T ($\gamma\gamma$-induced final states are peaked at small p_T). The contribution to other large-Q^2 DY configurations, such as inclusive production at large p_T, is suppressed.

The excellent agreement between theory and data, at the few percent level, is shown in the right plot of Fig. 6, from a recent analysis of the CMS experiment.[33]

3. Multiple Production of Vector Bosons

Pair production of gauge bosons includes contributions from channels like $f\bar{f} \to \gamma/Z^* \to W^+W^-$ (with e.g. $f = e, q$), which probe directly gauge boson self-interactions, and are sensitive to deviations from the SM value of the relevant couplings (deviations known as "anomalous couplings"). Until recently the most accurate studies of these couplings came from LEP2 data above the WW threshold. In hadron colliders, one can explore a much broader range of momentum scales and of off-shell configurations (e.g. probing channels such as $q\bar{q}' \to W^* \to W\gamma$). The limited statistics and kinematical reach available at the Tevatron is nowadays largely surpassed at the LHC, whose sensitivity to anomalous couplings is quickly overtaking that of LEP2. The LHC will also have sensitivity to quartic gauge interactions, via the contributions to the $VV \to VV$ amplitude in the vector boson scattering processes $qq \to qqVV$.

Table 1.   Production cross sections (pb) in pp collisions at 13 TeV for processes with multiple vector boson final states, from Ref. 77.

$W^{\pm}$	Z^0	W^+W^-	$W^{\pm}Z^0$	Z^0Z^0	$W^+W^-W^{\pm}$	$W^+W^-Z^0$
$1.7 \cdot 10^5$	$5.4 \cdot 10^4$	$1.0 \cdot 10^2$	$4.5 \cdot 10^1$	$1.4 \cdot 10^1$	$2.1 \cdot 10^{-1}$	$1.7 \cdot 10^{-1}$
$W^{\pm}Z^0Z^0$	$Z^0Z^0Z^0$	$W^+W^-W^+W^-$	$W^+W^-W^{\pm}Z^0$	$W^+W^-Z^0Z^0$	$W^{\pm}Z^0Z^0Z^0$	$Z^0Z^0Z^0Z^0$
$5.6 \cdot 10^{-2}$	$1.4 \cdot 10^{-2}$	$1.0 \cdot 10^{-3}$	$1.2 \cdot 10^{-3}$	$7.1 \cdot 10^{-4}$	$1.2 \cdot 10^{-4}$	$2.6 \cdot 10^{-5}$

Table 2.   Cross section ratios in pp collisions at 13 TeV for processes with multiple vector boson final states.

$W^{\pm}/Z^0$	$W^+W^-/W^{\pm}Z^0$	$W^+W^-W^{\pm}/W^+W^-Z^0$	$W^+W^-W^+W^-/$ $W^+W^-W^{\pm}Z^0$
3.1	2.2	1.2	0.8
$W^+W^-/W^{\pm}$	$W^{\pm}W^+W^-/W^+W^-$	$W^+W^-W^+W^-/W^+W^-W^{\pm}$	
$0.6 \cdot 10^{-3}$	$2.1 \cdot 10^{-3}$	$4.8 \cdot 10^{-3}$	

Final states with gauge boson pairs are also fundamental signatures of Higgs decays, $H \to ZZ^*$ and $H \to WW^*$. The direct VV production is an important background to the isolation of these Higgs signals, as well as to the signals of associated Higgs production, $pp \to VH$, where Higgs decays such as $H \to b\bar{b}$ or $H \to \tau^+\tau^-$ are subject to the background coming from the tail of the Z^0 invariant mass distribution in $pp \to VZ^0$.

Furthermore, as a source of multilepton final states, multiple gauge boson production is a potential background to a large number of BSM searches, for example searches for the supersymmetric partners of gauge and Higgs bosons.

Table 1 collects the NLO production rates for all processes with up to four massive gauge bosons in the final state, taken from the comprehensive tabulation of NLO results for high-multiplicity final states in Ref. 77, which also lists the respective systematic uncertainties. Most of these processes should be eventually measurable at the LHC. The ratio $\sigma(W^{\pm})/\sigma(Z^0) \sim 3$ (see Table 2) turns out to be rather independent of the energy, and of whether we consider pp or $p\bar{p}$ collisions. When considering leptonic final states, this leads to the well know factor of $\sigma(W^{\pm})BR(W \to \ell\nu)/\sigma(Z^0)BR(Z \to \ell^+\ell^-) \sim 10$, which was observed at the S$p\bar{p}$S, at the Tevatron and at the LHC. This ratio reflects primarily the nature and value of the couplings of W and Z bosons to the up and down quarks in the proton. When the number of final-state gauge bosons increases, the relative emission rate of further W or Z bosons gets closer to 1, as gauge boson selfcouplings become dominant with respect to the couplings to initial state quarks. This is seen, for example, in the first row of Table 2. Notice, finally, that the cost of emitting additional gauge bosons decreases with multiplicity: in part this is due to the larger number of sources to

Table 3. W^+W^- cross sections measured in pp collisions at 7 and 8 TeV. The first three measurements include the Higgs contribution, the fourth one subtracts it. NLO and NNLO theoretical predictions are from Ref. 79. The $gg \to WW$ process is included only in the NNLO contribution, and the Higgs contribution,[80] to be added to the NNLO result for the comparison with the data in the first three rows, is shown separately.

Experiment	Data (pb)	NLO	NNLO	$gg \to H \to WW^*$
ATLAS[81] (7 TeV, incl. H)	54.4 ± 6.0	$45.2^{+1.7}_{-1.3}$	$49.0^{+1.0}_{-0.9}$	$3.3^{+0.2}_{0.3}$
CMS[82] (7 TeV, incl. H)	52.4 ± 5.1			
ATLAS[83] (8 TeV, incl. H)	$71.4 \pm 1.2_{\text{stat}}\,^{+5.6}_{-5.0}\,_{\text{tot}}$	$54.8^{+2.0}_{-1.6}$	$59.8^{+1.3}_{-1.1}$	$4.1^{+0.3}_{-0.3}$
CMS[84] (8 TeV, no H)	$60.1 \pm 0.9_{\text{stat}} \pm 3.1_{\text{th}}$ $\pm 3.5_{\text{exp+lum}}$			

couple to, in part to the reduced relative increase in required energy (producing two gauge boson takes at least twice the energy than producing one, while producing four takes only an extra 30% more than producing 3).

At this time, the only final states measured with large statistics are those with two bosons (for a complete phenomenological study of boson pair production at the LHC, see e.g. Ref. 78). In the case of W^+W^- production, in particular, the statistical uncertainty of the LHC measurements at 8 TeV is already about half the size of the systematics one. Table 3 summarises the status of comparisons between data and theory for this channel. The consistency of theoretical predictions and data is greatly improved by the inclusion of the NNLO results.[79,c] While compatible with uncertainties, some small discrepancy is nevertheless present at 8 TeV, even between experimental results. New measurements at 13 TeV, and in particular the potentially more accurate measurement of cross section ratios[88] between 13 and 8 TeV, will certainly clarify the whole picture.

On the theoretical side, note that at $\mathcal{O}(\alpha_s^2)$ a new contribution appears, namely $gg \to WW$, mediated by a quark loop (since this gg channel enters for the first time at this order, its description is referred to as LO even though it enters through a loop diagram). Its size is significant, due to the large gg luminosity, and contributes toward improving the agreement between theory and data. The NLO correction to this new channel (therefore of $\mathcal{O}(\alpha_s^3)$) has recently been computed.[89] At the LHC, the correction relative to the LO $gg \to WW$ process can be large, up to 50%, leading to a further increase of the total cross section by about 2%. But the size of the cross section depends strongly on the kinematical cuts applied to the final state,[89] an element that should be taken into proper account in the comparison with the experimental measurements. This underscores the complexity of such high-precision tests of QCD dynamics, but it is encouraging that continuous progress is taking place in improving the theoretical calculations.

---

[c]A similar pattern is observed in the case of the $V\gamma$ production cross sections, where the very recent completion of the NNLO calculations[85] has improved the agreement with LHC data.[86,87]

4. Associated Production of Vector Bosons with Jets and Heavy Quarks

The associated production of gauge bosons and jets[90] is a natural manifestation of higher-order QCD corrections to inclusive production. The measurement of such final states has a long history, starting from the CERN S$p\bar{p}$S collider experiments,[91–93] which highlighted their role as backgrounds to new physics, and as a probe of α_S. Later studies at the Tevatron[94,95] have been crucial to test quantitatively the theoretical modelling, and to establish background rates for the discovery and study of the top quark and for the search of the Higgs boson. On the theory side, the last few years have seen remarkable progress, with the NLO calculations[96–101] of processes with up to 5 jets, the inclusion of NLO EW[102] corrections, and most recently of NNLO QCD corrections to $W + 1$ jet[103] and $Z + 1$ jet[104] production.

The latest LHC measurements[105–108] of $V+$ multijet production have reached multiplicities up to 7 jets, with a precision and an agreement with theoretical calculations that, at least for multiplicities up to 4 jets and for most kinematical distributions, reach the level of $\pm(10-20)\%$. This is shown for example in Fig. 7. Notice that a new feature of the production of gauge bosons with jets emerges at the LHC, given the large jet energies that can be reached: the probability of weak
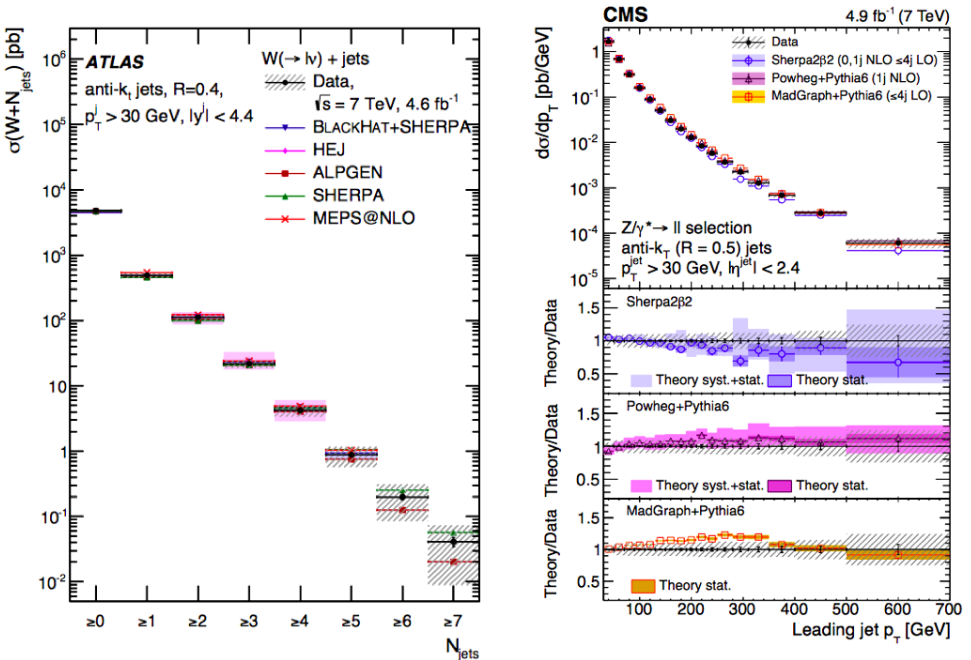

Fig. 7. Data vs. theory comparison for $V+$jets at the LHC. Left: $W + N$ jet rates at 7 TeV.[105] Right: leading-jet p_T spectrum in $Z+$jets at 7 TeV.[108]
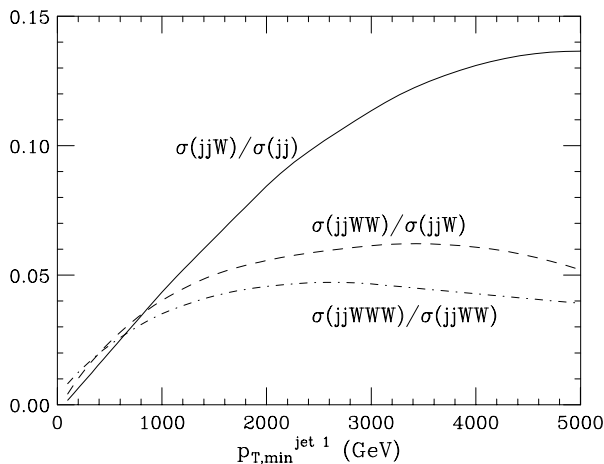
Fig. 8.   Emission probability for W bosons at 14 TeV, in events with 2 or more jets where the leading jet has $p_T > p_{T,\min}$.

boson emission increases, from the 10^{-3} level of inclusive QCD processes, up to over 10% for jet transverse momenta of several TeV (see Fig. 8).

4.1. $W+charm\ quarks$

At the LO, the W+charm cross section is proportional to $\sin^2 \theta_C d(x) + \cos^2 \theta_C s(x)$, where $d(x)$ and $s(x)$ are the PDFs of the down and strange quarks and θ_C is the Cabibbo mixing angle. The Cabibbo-allowed process is dominant, and allows the measurement of the strange quark distribution.[110,111] The difference in the production rate of W^-c and $W^+\bar{c}$, after accounting for the small contribution of d and $\bar{d}$ quarks, is furthermore sensitive to the difference between $s(x)$ and $\bar{s}(x)$.[d] The first measurements at the LHC[112–114] have already led to useful constraints on PDF fits, but are still statistics limited, and there is still large room for improvements.

4.2. $V + Q\bar{Q}$, with $Q = c, b$

The associated production of vector bosons and heavy quark pairs is an interesting SM process, which has particular relevance as leading background to studies of the top quark, of the Higgs boson, and to many searches for physics beyond the SM. While the case of $c\bar{c}$ and $b\bar{b}$ production are similar from the theoretical point of view, we shall focus here on the case of b pairs, which has a larger phenomenological relevance, and for which more experimental data are available.

---

[d]The assumption $s(x) = \bar{s}(x)$, which has been used in the past in global PDF fits due to the lack of direct experimental discriminating observables, is not respected at the NNLO in the Q^2 evolution of PDFs.

$Wb\bar{b}$ + jets production gives rise to final states similar to those arising from $t\bar{t}$ production, and its presence, particularly at the Tevatron, was one of the main hurdles in the top quark discovery and in its precision studies. This is less so at the LHC, where its rate relative to the $t\bar{t}$ signal is much smaller than at the Tevatron. $Vb\bar{b}$ is an irreducible background to the associated production of gauge and Higgs bosons, in the leading Higgs decay channel $VH \to Vb\bar{b}$. As such, its understanding is nowadays the subject of many studies.

From the theoretical perspective, the Wbb and Zbb processes are rather different. In the former case, the only LO production channel is $q\bar{q}' \to Wb\bar{b}$. In the latter case, both $q\bar{q}$ and gg initial states contribute to the $Zb\bar{b}$ production. For $q\bar{q} \to Vb\bar{b}$, the $b\bar{b}$ pair is produced by the splitting of a final state gluon in the $q\bar{q} \to Vg$ process. The difference between $q\bar{q}$- and gg-initiated processes is particularly relevant when one considers final states where only one b jet is tagged: in the $gg \to Zb(\bar{b})$ case, in fact, there is a large contribution induced by processes in which one of the gluons in $gg \to Zbb$ undergoes a collinear splitting to $b\bar{b}$, and the b quark undergoes a hard scattering with the other gluon ($gb \to Zb$), leading to the high-p_T tagged b-jet. The $\bar{b}$ is preferentially emitted at small p_T, covering a wide rapidity range, and the integral over its full emission phase space leads to a large logarithm. One could describe this process by associating this large logarithm to the build up of a b quark PDF inside the proton, and the measurement of Zb final states provides therefore a powerful probe for the determination of the b PDF. In the case of $q\bar{q} \to Wbb$, on the other hand, the measurement of single b-jet production receives comparable contributions from the cases where the $\bar{b}$ is too soft to reconstruct a jet, and cases in which the pair produced by gluon splitting is collinear, and is merged within the same jet. In the latter case, one exposes potentially large logarithms $\log(p_T^{\text{jet}}/m_b)$.

For what concerns the comparison of theory and data from the Tevatron[118–120] and from the LHC,[114,121–125] the agreement of data for $V + b$-jet with NLO fixed-order perturbative calculations[115–117] is often marginal (possibly due to the presence of large logarithms that call for improved resummed calculations), although consistent with the uncertainties. A better agreement is typically found in the comparisons with data where both b-jets are tagged. Future measurements at the LHC, with larger statistics and better control on the experimental systematics, will allow further improvements of the theoretical modelling.

4.3. $V + t\bar{t}$

The associated production of W and Z bosons with a pair of top quarks is a special case of the processes discussed in the previous subsection. In many respects, the theoretical description of $Vt\bar{t}$ production is however simpler: the mass of the top quark and of the gauge bosons are both large and of comparable size, so that we do not have the difficulties associated with the presence of largely different scales. For example, there are no large logarithms to be resummed, or assumptions to be made

Table 4. Production cross sections (pb) in *pp* collisions at 13 TeV for various top quark and vector boson final states, from Ref. 77.

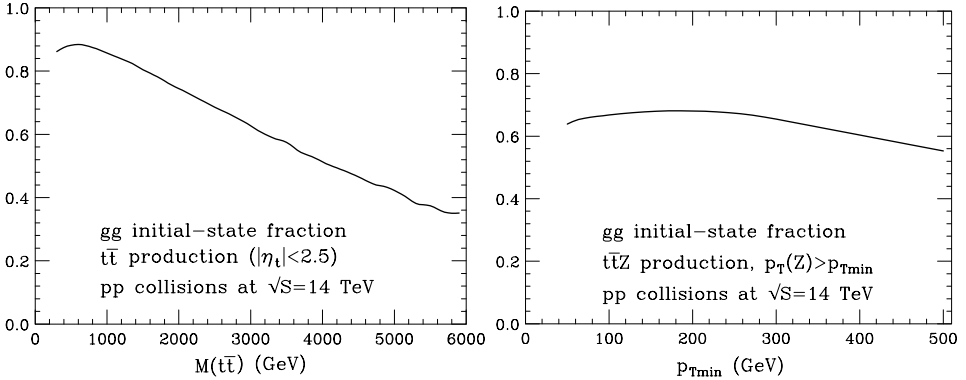| $t\bar{t}$	$t\bar{t}W^{\pm}$	$t\bar{t}Z^0$	$t\bar{t}W^+W^-$	$t\bar{t}W^{\pm}Z^0$	$t\bar{t}Z^0Z^0$
674	0.57	0.76	$9.9 \cdot 10^{-3}$	$3.5 \cdot 10^{-3}$	$1.8 \cdot 10^{-3}$

Fig. 9. Initial state *gg* fraction in inclusive production of $t\bar{t}$ (left) and $Zt\bar{t}$ (right), in *pp* collisions at $\sqrt{S} = 14$ TeV.

about the relevant heavy quark density of the proton; furthermore, the prediction for the basic process, namely the inclusive production of the heavy quark pair, is much more precise for top quarks than for bottom or charm quarks.

From the phenomenological perspective, the associated production with top quarks has interesting features. To start with, at LHC energies and above these processes are the main source of multiple gauge boson production. This is clear from Table 4, which reports the total rates for several final states involving top quarks and massive gauge bosons. Considering that each top and antitop quark produces a W boson in their decay, the comparison with the multi-V rates given in Table 1 shows that final states with W^+W^- pairs are more likely to arise from $t\bar{t}$ production and decay than from direct EW production. This is true as well of processes with production of additional gauge bosons, e.g. $t\bar{t}Z$ versus W^+W^-Z. This fact should be taken into account when extracting EW production rates from the data, and when estimating multiboson backgrounds to BSM signals.

Another interesting observation is that, in *pp* collisions at the LHC energies and above, the production of a Z boson is more frequent than the production of a W boson, contrary to the usual hierarchy of W vs. Z production rates. The reason is that, at LO, the $t\bar{t}W$ final state can only be produced starting from the $q\bar{q}'$ initial state, while $t\bar{t}Z$ can be produced from both $q\bar{q}$ and gg initial states. The gg fraction in $t\bar{t}Z$ production at 14 TeV is shown in Fig. 9, as a function of $p_{T,Z}$. Since inclusive $t\bar{t}$ production is dominated by the gg channel (85% of the rate at $\sqrt{S} = 14$ TeV, see also the left plot in Fig. 9), the emission of a W is suppressed with respect to

the emission of a Z. This is shown explicitly in Table 4, where the rates of various processes with top quarks and gauge bosons are given. The usual hierarchy in rate between W and Z production is restored for associated production of W^+W^- versus ZZ, when the gg initial state is active for both processes.

The above considerations have several corollaries. The production of a W boson, singling out the $q\bar{q}'$ initial state, allows to scrutinise more closely the production mechanism $q\bar{q} \to t\bar{t}$, which is otherwise suppressed at the LHC. This may be useful[126] to enhance the sensitivity to possible new physics at the origin of the forward-backward production asymmetry reported at the Tevatron.[127–129] The study of $t\bar{t}W$ production at very large invariant mass of the $t\bar{t}$ system, furthermore, allows to probe directly the $t\bar{t}g$ vertex in the domain of gluon virtuality $Q \sim m_{tt}$. This is because the leading production diagram has a W emitted from the initial state, followed by the s-channel annihilation $q\bar{q} \to t\bar{t}$.

The final state $t\bar{t}Z$, on the other hand, allows to measure directly the $t\bar{t}Z$ vertex, since this is the coupling that drives the dominant $gg \to t\bar{t}Z$ contribution.[130] Future LHC data will allow to set stringent and model-independent limits on anomalous dipole contributions to the $t\bar{t}Z$ vertex, with sensitivity comparable to that obtained from indirect EW precision measurements at LEP.[131]

Both $t\bar{t}W$ and $t\bar{t}Z$ processes are known theoretically with full NLO accuracy in QCD,[132–135] which leads to an intrinsic systematic uncertainty of about $\pm 10\%$. In spite of low production rates at the energies of the first run of the LHC ($\sigma(t\bar{t}W^\pm) \sim \sigma(t\bar{t}Z) \sim 200 \pm 20$ fb at $\sqrt{S} = 8$ TeV), ATLAS and CMS have nevertheless obtained a signal evidence, for both processes, at the level of 5σ, or better. The first CMS results[136] have been updated recently,[137] leading to the measurements of $\sigma(t\bar{t}W^\pm) = 382^{+117}_{-102}$ fb (4.8σ) and $\sigma(t\bar{t}Z) = 242^{+65}_{-55}$ fb (6.4σ). ATLAS[138] measured $\sigma(t\bar{t}W^\pm) = 369^{+100}_{-91}$ fb (5.0σ) and $\sigma(t\bar{t}Z) = 176^{+58}_{-52}$ fb (4.2σ). All these results are well compatible with the SM predictions.

5. Conclusions

The production of vector gauge bosons in hadron collisions is like a Swiss knife: it is a versatile, reliable and robust tool for physics at the high-energy frontier. It exposes a vast variety of phenomena, covering most aspects of the dynamics of both EW and strong interactions. While contributing to our deeper understanding and consolidation of the SM, the knowledge acquired about the production mechanisms of gauge bosons is also essential to study the properties of the top quark and of the Higgs boson, and to refine the sensitivity of searches for BSM phenomena.

The precision of measurements and theoretical calculations has greatly improved in the past few years, and allows now comparisons of gauge boson production properties at the few percent level of precision. This precision is superior to what can be achieved in most other hard processes in hadronic collisions, and is liable to improve even further, through continued theoretical and experimental efforts and additional

ingenuity. Already today, this precision can be used to improve the determination of the EW parameters and of the proton PDFs, competing with the pre-LHC state-of-the-art provided, respectively, by the results of the LEP and SLC e^+e^- colliders, and of the HERA *ep* collider. It is easy to predict that the physics of W and Z bosons at the LHC will continue surprising us for its richness for a long time to come.

References

1. G. Arnison *et al.* [UA1 Collaboration], *Phys. Lett. B* **122**, 103 (1983).
2. M. Banner *et al.* [UA2 Collaboration], *Phys. Lett. B* **122**, 476 (1983).
3. G. Arnison *et al.* [UA1 Collaboration], *Phys. Lett. B* **126**, 398 (1983).
4. P. Bagnaia *et al.* [UA2 Collaboration], *Phys. Lett. B* **129**, 130 (1983).
5. G. Aad *et al.* [ATLAS Collaboration], *Phys. Lett. B* **716**, 1 (2012) [arXiv:1207.7214 [hep-ex]].
6. S. Chatrchyan *et al.* [CMS Collaboration], *Phys. Lett. B* **716**, 30 (2012) [arXiv: 1207.7235 [hep-ex]].
7. S. D. Drell and T. M. Yan, *Phys. Rev. Lett.* **25**, 316 (1970) [*Phys. Rev. Lett.* **25**, 902 (1970)].
8. T. A. Aaltonen *et al.* [CDF and D0 Collaborations], *Phys. Rev. D* **88**, 5, 052018 (2013) [arXiv:1307.7627 [hep-ex]].
9. R. Hamberg, W. L. van Neerven and T. Matsuura, *Nucl. Phys. B* **359**, 343 (1991) [*Nucl. Phys. B* **644**, 403 (2002)].
10. R. V. Harlander and W. B. Kilgore, *Phys. Rev. Lett.* **88**, 201801 (2002) [hep-ph/0201206].
11. C. Anastasiou, L. J. Dixon, K. Melnikov and F. Petriello, *Phys. Rev. D* **69**, 094008 (2004) [hep-ph/0312266].
12. K. Melnikov and F. Petriello, *Phys. Rev. D* **74**, 114017 (2006) [hep-ph/0609070].
13. S. Catani, L. Cieri, G. Ferrera, D. de Florian and M. Grazzini, *Phys. Rev. Lett.* **103**, 082001 (2009) [arXiv:0903.2120 [hep-ph]].
14. R. Gavin, Y. Li, F. Petriello and S. Quackenbush, *Comput. Phys. Commun.* **182**, 2388 (2011) [arXiv:1011.3540 [hep-ph]].
15. A. Karlberg, E. Re and G. Zanderighi, *JHEP* **1409**, 134 (2014) [arXiv:1407.2940 [hep-ph]].
16. S. Höche, Y. Li and S. Prestel, *Phys. Rev. D* **91**, 7, 074015 (2015) [arXiv:1405.3607 [hep-ph]].
17. S. Alioli, C. W. Bauer, C. Berggren, F. J. Tackmann and J. R. Walsh, *Phys. Rev. D* **92**, 9, 094020 (2015) [arXiv:1508.01475 [hep-ph]].
18. S. Dittmaier and M. Kramer, *Phys. Rev. D* **65**, 073007 (2002) [hep-ph/0109062].
19. U. Baur and D. Wackeroth, *Phys. Rev. D* **70**, 073015 (2004) [hep-ph/0405191].
20. U. Baur, O. Brein, W. Hollik, C. Schappacher and D. Wackeroth, *Phys. Rev. D* **65**, 033007 (2002) [hep-ph/0108274].
21. Y. Li and F. Petriello, *Phys. Rev. D* **86**, 094034 (2012) [arXiv:1208.5967 [hep-ph]].
22. S. Dittmaier, A. Huss and C. Schwinn, arXiv:1511.08016 [hep-ph].
23. S. Forte and G. Watt, *Ann. Rev. Nucl. Part. Sci.* **63**, 291 (2013) [arXiv:1301.6754 [hep-ph]].
24. G. Aad *et al.* [ATLAS Collaboration], *Phys. Rev. D* **85**, 072004 (2012) [arXiv:1109.5141 [hep-ex]].

25. S. Chatrchyan *et al.* [CMS Collaboration], *JHEP* **1110**, 132 (2011) [arXiv:1107.4789 [hep-ex]].
26. R. Aaij *et al.* [LHCb Collaboration], *JHEP* **1412**, 079 (2014) [arXiv:1408.4354 [hep-ex]].
27. T. Aaltonen *et al.* [CDF Collaboration], *Phys. Rev. Lett.* **102**, 181801 (2009) [arXiv:0901.2169 [hep-ex]].
28. S. Catani, G. Ferrera and M. Grazzini, *JHEP* **1005**, 006 (2010) [arXiv:1002.3115 [hep-ph]].
29. R. Gavin, Y. Li, F. Petriello and S. Quackenbush, *Comput. Phys. Commun.* **184**, 208 (2013) [arXiv:1201.5896 [hep-ph]].
30. V. M. Abazov *et al.* [D0 Collaboration], *Phys. Rev. D* **91**, 3, 032007 (2015) [*Phys. Rev. D* **91**, 7, 079901 (2015)] [arXiv:1412.2862 [hep-ex]].
31. G. Aad *et al.* [ATLAS Collaboration], *Phys. Lett. B* **701**, 31 (2011) [arXiv:1103.2929 [hep-ex]].
32. S. Chatrchyan *et al.* [CMS Collaboration], *Phys. Rev. D* **90**, 3, 032004 (2014) [arXiv:1312.6283 [hep-ex]].
33. V. Khachatryan *et al.* [CMS Collaboration], *Eur. Phys. J. C* **75**, 4, 147 (2015) [arXiv:1412.1115 [hep-ex]].
34. S. Alekhin, J. Bluemlein and S. Moch, *Phys. Rev. D* **89**, 5, 054028 (2014) [arXiv:1310.3059 [hep-ph]].
35. R. D. Ball *et al.* [NNPDF Collaboration], *JHEP* **1504**, 040 (2015) [arXiv:1410.8849 [hep-ph]].
36. L. A. Harland-Lang, A. D. Martin, P. Motylinski and R. S. Thorne, *Eur. Phys. J. C* **75**, 5, 204 (2015) [arXiv:1412.3989 [hep-ph]].
37. S. Dulat *et al.*, arXiv:1506.07443 [hep-ph].
38. S. Farry and R. Gauld, arXiv:1505.01399 [hep-ph].
39. R. D. Ball, V. Bertone, F. Cerutti, L. Del Debbio, S. Forte, A. Guffanti, J. I. Latorre and J. Rojo *et al.*, *Nucl. Phys. B* **849**, 296 (2011) [arXiv:1101.1300 [hep-ph]].
40. J. Gao, M. Guzzi, J. Huston, H. L. Lai, Z. Li, P. Nadolsky, J. Pumplin and D. Stump *et al.*, *Phys. Rev. D* **89**, 3, 033009 (2014) [arXiv:1302.6246 [hep-ph]].
41. R. Aaij *et al.* [LHCb Collaboration], *JHEP* **1508**, 039 (2015) [arXiv:1505.07024 [hep-ex]].
42. R. Aaij *et al.* [LHCb Collaboration], arXiv:1503.00963 [hep-ex].
43. R. Aaij *et al.* [LHCb Collaboration], arXiv:1511.08039 [hep-ex].
44. S. Schael *et al.* [ALEPH and DELPHI and L3 and OPAL and SLD and LEP Electroweak Working Group and SLD Electroweak Group and SLD Heavy Flavour Group Collaborations], *Phys. Rept.* **427**, 257 (2006) [hep-ex/0509008].
45. T. A. Aaltonen *et al.* [CDF Collaboration], *Phys. Rev. D* **89**, 7, 072005 (2014) [arXiv:1402.2239 [hep-ex]].
46. S. Yang *et al.* (D0 Collaboration), D0 Note 6426-CONF 2014.
47. S. Chatrchyan *et al.* [CMS Collaboration], *Phys. Rev. D* **84**, 112002 (2011) [arXiv:1110.2682 [hep-ex]].
48. G. Aad *et al.* [ATLAS Collaboration], arXiv:1503.03709 [hep-ex].
49. R. Aaij *et al.* [LHCb Collaboration], arXiv:1509.07645 [hep-ex].
50. J. Rojo *et al.*, *J. Phys. G* **42**, 103103 (2015) [arXiv:1507.00556 [hep-ph]].
51. J. Kubar-Andre and F. E. Paige, *Phys. Rev. D* **19**, 221 (1979).
52. G. Altarelli, R. K. Ellis and G. Martinelli, *Nucl. Phys. B* **143**, 521 (1978) [*Nucl. Phys. B* **146**, 544 (1978)].
53. G. Altarelli, R. K. Ellis and G. Martinelli, *Nucl. Phys. B* **157**, 461 (1979).
54. Y. L. Dokshitzer, D. Diakonov and S. I. Troian, *Phys. Rept.* **58**, 269 (1980).

55. G. Parisi and R. Petronzio, *Nucl. Phys. B* **154**, 427 (1979).
56. G. Curci, M. Greco and Y. Srivastava, *Nucl. Phys. B* **159**, 451 (1979).
57. J. C. Collins and D. E. Soper, *Nucl. Phys. B* **193**, 381 (1981) [*Nucl. Phys. B* **213**, 545 (1983)].
58. C. Balazs and C. P. Yuan, *Phys. Rev. D* **56**, 5558 (1997) [hep-ph/9704258].
59. G. Bozzi, S. Catani, G. Ferrera, D. de Florian and M. Grazzini, *Phys. Lett. B* **696**, 207 (2011) [arXiv:1007.2351 [hep-ph]].
60. T. Becher, M. Neubert and D. Wilhelm, *JHEP* **1202**, 124 (2012) [arXiv:1109.6027 [hep-ph]].
61. V. M. Abazov *et al.* [D0 Collaboration], *Phys. Rev. Lett.* **106**, 122001 (2011) [arXiv:1010.0262 [hep-ex]].
62. R. K. Ellis, G. Martinelli and R. Petronzio, *Nucl. Phys. B* **211**, 106 (1983).
63. G. Altarelli, R. K. Ellis, M. Greco and G. Martinelli, *Nucl. Phys. B* **246**, 12 (1984).
64. R. J. Gonsalves, J. Pawlowski and C. F. Wai, *Phys. Rev. D* **40**, 2245 (1989).
65. P. B. Arnold and M. H. Reno, *Nucl. Phys. B* **319**, 37 (1989) [*Nucl. Phys. B* **330**, 284 (1990)].
66. S. Catani, D. de Florian, G. Ferrera and M. Grazzini, arXiv:1507.06937 [hep-ph].
67. S. A. Malik and G. Watt, *JHEP* **1402**, 025 (2014) [arXiv:1304.2424 [hep-ph]].
68. G. Aad *et al.* [ATLAS Collaboration], *JHEP* **1409**, 145 (2014) [arXiv:1406.3660 [hep-ex]].
69. V. Khachatryan *et al.* [CMS Collaboration], arXiv:1504.03511 [hep-ex].
70. M. Guzzi, P. M. Nadolsky and B. Wang, *Phys. Rev. D* **90**, 1, 014030 (2014) [arXiv:1309.1393 [hep-ph]].
71. A. Banfi, M. Dasgupta, S. Marzani and L. Tomlinson, *Phys. Lett. B* **715**, 152 (2012) [arXiv:1205.4760 [hep-ph]].
72. A. Denner, S. Dittmaier, T. Kasprzik and A. Muck, *JHEP* **1106**, 069 (2011) [arXiv:1103.0914 [hep-ph]].
73. K. Hagiwara, R. D. Peccei, D. Zeppenfeld and K. Hikasa, *Nucl. Phys. B* **282**, 253 (1987).
74. U. Baur and E. L. Berger, *Phys. Rev. D* **47**, 4889 (1993).
75. R. Boughezal, Y. Li and F. Petriello, *Phys. Rev. D* **89**, 3, 034030 (2014) [arXiv:1312.3972 [hep-ph]].
76. R. D. Ball *et al.* [NNPDF Collaboration], *Nucl. Phys. B* **877**, 290 (2013) [arXiv:1308.0598 [hep-ph]].
77. J. Alwall, R. Frederix, S. Frixione, V. Hirschi, F. Maltoni, O. Mattelaer, H.-S. Shao and T. Stelzer *et al.*, *JHEP* **1407**, 079 (2014) [arXiv:1405.0301 [hep-ph]].
78. J. M. Campbell, R. K. Ellis and C. Williams, *JHEP* **1107**, 018 (2011) [arXiv:1105.0020 [hep-ph]].
79. T. Gehrmann, M. Grazzini, S. Kallweit, P. Maierhfer, A. von Manteuffel, S. Pozzorini, D. Rathlev and L. Tancredi, *Phys. Rev. Lett.* **113**, 21, 212001 (2014) [arXiv:1408.5243 [hep-ph]].
80. S. Heinemeyer *et al.* [LHC Higgs Cross Section Working Group Collaboration], arXiv:1307.1347 [hep-ph].
81. G. Aad *et al.* [ATLAS Collaboration], *Phys. Lett. B* **712**, 289 (2012) [arXiv:1203.6232 [hep-ex]].
82. S. Chatrchyan *et al.* [CMS Collaboration], *Eur. Phys. J. C* **73**, 10, 2610 (2013) [arXiv:1306.1126 [hep-ex]].
83. The ATLAS Collaboration, ATLAS-CONF-2014-033, ATLAS-COM-CONF-2014-045.
84. CMS Collaboration [CMS Collaboration], CMS-PAS-SMP-14-016.

85. M. Grazzini, S. Kallweit and D. Rathlev, arXiv:1504.01330 [hep-ph].
86. G. Aad *et al.* [ATLAS Collaboration], *Phys. Rev. D* **87**, 11, 112003 (2013) [*Phys. Rev. D* **91**, 11, 119901 (2015)] [arXiv:1302.1283 [hep-ex]].
87. V. Khachatryan *et al.* [CMS Collaboration], *JHEP* **1504**, 164 (2015) [arXiv:1502.05664 [hep-ex]].
88. M. L. Mangano and J. Rojo, *JHEP* **1208**, 010 (2012) [arXiv:1206.3557 [hep-ph]].
89. F. Caola, K. Melnikov, R. Rntsch and L. Tancredi, arXiv:1511.08617 [hep-ph].
90. J. Campbell and M. Mangano, *Ann. Rev. Nucl. Part. Sci.* **61**, 311 (2011).
91. G. Arnison *et al.* [UA1 Collaboration], *Phys. Lett. B* **147**, 493 (1984).
92. P. Bagnaia *et al.* [Bern-CERN-Copenhagen-Orsay-Pavia-Saclay and UA2 Collaborations], *Phys. Lett. B* **139**, 105 (1984).
93. R. Ansari *et al.* [UA2 Collaboration], *Phys. Lett. B* **215**, 175 (1988).
94. T. Aaltonen *et al.* [CDF Collaboration], *Phys. Rev. D* **77**, 011108 (2008) [arXiv:0711.4044 [hep-ex]].
95. V. M. Abazov *et al.* [D0 Collaboration], *Phys. Rev. D* **88**, 9, 092001 (2013) [arXiv:1302.6508 [hep-ex]].
96. R. K. Ellis, K. Melnikov and G. Zanderighi, *Phys. Rev. D* **80**, 094002 (2009) [arXiv:0906.1445 [hep-ph]].
97. C. F. Berger, Z. Bern, L. J. Dixon, F. Febres Cordero, D. Forde, T. Gleisberg, H. Ita and D. A. Kosower *et al.*, *Phys. Rev. D* **80**, 074036 (2009) [arXiv:0907.1984 [hep-ph]].
98. C. F. Berger, Z. Bern, L. J. Dixon, F. Febres Cordero, D. Forde, T. Gleisberg, H. Ita and D. A. Kosower *et al.*, *Phys. Rev. D* **82**, 074002 (2010) [arXiv:1004.1659 [hep-ph]].
99. C. F. Berger, Z. Bern, L. J. Dixon, F. Febres Cordero, D. Forde, T. Gleisberg, H. Ita and D. A. Kosower *et al.*, *Phys. Rev. Lett.* **106**, 092001 (2011) [arXiv:1009.2338 [hep-ph]].
100. H. Ita, Z. Bern, L. J. Dixon, F. Febres Cordero, D. A. Kosower and D. Maitre, *Phys. Rev. D* **85**, 031501 (2012) [arXiv:1108.2229 [hep-ph]].
101. Z. Bern, L. J. Dixon, F. Febres Cordero, S. Hche, H. Ita, D. A. Kosower, D. Matre and K. J. Ozeren, *Phys. Rev. D* **88**, 1, 014025 (2013) [arXiv:1304.1253 [hep-ph]].
102. A. Denner, S. Dittmaier, T. Kasprzik and A. Muck, *JHEP* **0908**, 075 (2009) [arXiv:0906.1656 [hep-ph]].
103. R. Boughezal, C. Focke, X. Liu and F. Petriello, arXiv:1504.02131 [hep-ph].
104. A. Gehrmann-De Ridder, T. Gehrmann, E. W. N. Glover, A. Huss and T. A. Morgan, arXiv:1507.02850 [hep-ph].
105. G. Aad *et al.* [ATLAS Collaboration], *Eur. Phys. J. C* **75**, 2, 82 (2015) [arXiv:1409.8639 [hep-ex]].
106. V. Khachatryan *et al.* [CMS Collaboration], *Phys. Lett. B* **741**, 12 (2015) [arXiv:1406.7533 [hep-ex]].
107. G. Aad *et al.* [ATLAS Collaboration], *JHEP* **1307**, 032 (2013) [arXiv:1304.7098 [hep-ex]].
108. V. Khachatryan *et al.* [CMS Collaboration], *Phys. Rev. D* **91**, 5, 052008 (2015) [arXiv:1408.3104 [hep-ex]].
109. G. Aad *et al.* [ATLAS Collaboration], *Eur. Phys. J. C* **74**, 12, 3168 (2014) [arXiv:1408.6510 [hep-ex]].
110. U. Baur, F. Halzen, S. Keller, M. L. Mangano and K. Riesselmann, *Phys. Lett. B* **318**, 544 (1993) [hep-ph/9308370].
111. W. T. Giele, S. Keller and E. Laenen, *Phys. Lett. B* **372**, 141 (1996) [hep-ph/9511449].
112. G. Aad *et al.* [ATLAS Collaboration], *JHEP* **1405**, 068 (2014) [arXiv:1402.6263 [hep-ex]].

113. S. Chatrchyan *et al.* [CMS Collaboration], *JHEP* **1402**, 013 (2014) [arXiv:1310.1138 [hep-ex]].
114. R. Aaij *et al.* [LHCb Collaboration], arXiv:1505.04051 [hep-ex].
115. J. M. Campbell, R. K. Ellis, F. Maltoni and S. Willenbrock, *Phys. Rev. D* **73**, 054007 (2006) [*Phys. Rev. D* **77**, 019903 (2008)] [hep-ph/0510362].
116. J. M. Campbell, R. K. Ellis, F. Maltoni and S. Willenbrock, *Phys. Rev. D* **75**, 054015 (2007) [hep-ph/0611348].
117. F. Febres Cordero, L. Reina and D. Wackeroth, *Phys. Rev. D* **80**, 034015 (2009) [arXiv:0906.1923 [hep-ph]].
118. T. Aaltonen *et al.* [CDF Collaboration], *Phys. Rev. D* **79**, 052008 (2009) [arXiv:0812.4458 [hep-ex]].
119. V. M. Abazov *et al.* [D0 Collaboration], *Phys. Rev. D* **87**, 9, 092010 (2013) [arXiv:1301.2233 [hep-ex]].
120. V. M. Abazov *et al.* [D0 Collaboration], *Phys. Rev. D* **91**, 5, 052010 (2015) [arXiv:1501.05325 [hep-ex]].
121. G. Aad *et al.* [ATLAS Collaboration], *JHEP* **1306**, 084 (2013) [arXiv:1302.2929 [hep-ex]].
122. S. Chatrchyan *et al.* [CMS Collaboration], *Phys. Lett. B* **735**, 204 (2014) [arXiv:1312.6608 [hep-ex]].
123. R. Aaij *et al.* [LHCb Collaboration], *JHEP* **1501**, 064 (2015) [arXiv:1411.1264 [hep-ex]].
124. G. Aad *et al.* [ATLAS Collaboration], *JHEP* **1410**, 141 (2014) [arXiv:1407.3643 [hep-ex]].
125. S. Chatrchyan *et al.* [CMS Collaboration], *JHEP* **1406**, 120 (2014) [arXiv:1402.1521 [hep-ex]].
126. F. Maltoni, M. L. Mangano, I. Tsinikos and M. Zaro, *Phys. Lett. B* **736**, 252 (2014) [arXiv:1406.3262 [hep-ph]].
127. T. Aaltonen *et al.* [CDF Collaboration], *Phys. Rev. D* **87**, 9, 092002 (2013) [arXiv:1211.1003 [hep-ex]].
128. V. M. Abazov *et al.* [D0 Collaboration], *Phys. Rev. D* **90**, 7, 072001 (2014) [arXiv:1403.1294 [hep-ex]].
129. J. A. Aguilar-Saavedra, D. Amidei, A. Juste and M. Perez-Victoria, arXiv:1406.1798 [hep-ph].
130. U. Baur, A. Juste, L. H. Orr and D. Rainwater, *Phys. Rev. D* **71**, 054013 (2005) [hep-ph/0412021].
131. R. Röntsch and M. Schulze, arXiv:1501.05939 [hep-ph].
132. A. Lazopoulos, T. McElmurry, K. Melnikov and F. Petriello, *Phys. Lett. B* **666**, 62 (2008) [arXiv:0804.2220 [hep-ph]].
133. A. Kardos, Z. Trocsanyi and C. Papadopoulos, *Phys. Rev. D* **85**, 054015 (2012) [arXiv:1111.0610 [hep-ph]].
134. J. M. Campbell and R. K. Ellis, *JHEP* **1207**, 052 (2012) [arXiv:1204.5678 [hep-ph]].
135. M. V. Garzelli, A. Kardos, C. G. Papadopoulos and Z. Trocsanyi, *JHEP* **1211**, 056 (2012) [arXiv:1208.2665 [hep-ph]].
136. V. Khachatryan *et al.* [CMS Collaboration], *Eur. Phys. J. C* **74**, 9, 3060 (2014) [arXiv:1406.7830 [hep-ex]].
137. V. Khachatryan *et al.* [CMS Collaboration], arXiv:1510.01131 [hep-ex].
138. G. Aad *et al.* [ATLAS Collaboration], arXiv:1509.05276 [hep-ex].